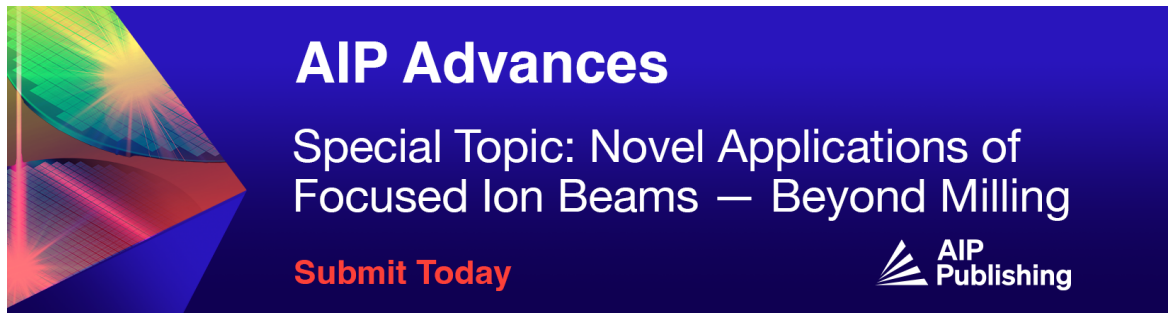# The screening effects of the screened exchange hybrid functional in surface systems: A case study on the CO/Pt(111) problem

H. Li; R. Gillen; J. Robertson

Check for updates

View Online

Export Citation

The screening effects of the screened exchange hybrid functional in surface systems: A case study on the CO/Pt(111) problem

H. Li,[1,a] R. Gillen,[2] and J. Robertson[3,b]

[1]*Department of Precision Instrument, Tsinghua University, Beijing, 100084, China*
[2]*Institut für Festkörperphysik. Technische Universität Berlin. Hardenbergstr. 36, 10623 Berlin, Germany*
[3]*Engineering Department, University of Cambridge, Cambridge CB2 1PZ, UK*

The screened exchange (sX) hybrid functional has been widely used in computational material science. Although it has widely been studied in bulk systems, less is known about its functional behavior in surface systems which are crucial to many technologies such as materials synthesis and nano-electronic devices. Assessing the screening dependent functional behaviors in the surface systems is therefore important for its application in such systems. In this work, we investigate the screening effects of the sX in CO adsorption on Pt(111) surface. The differences between the sX and Heyd-Scuseria-Ernzerhof (HSE06) hybrid functionals, and the effects of screening parameters are studied. The screening has two effects: first, the HOMO-LUMO gap is screening dependent. This affects the site preference most significantly. In this work, atop adsorption of CO/Pt(111) is predicted by the hybrid functionals with screened exchange potential. The sX(1.44) gives the largest HOMO-LUMO gap for the isolated CO molecule. The adsorption energy difference between the atop and fcc site is also the largest by the sX(1.44) which is explained by the reduced metal d states to the CO $2\pi^*$ state back-donation, with stronger effect for the fcc adsorption than for the atop adsorption; second, the adsorption energy is screening dependent. This can be seen by comparing the sX(2.38) and HSE06 which have different screening strengths. They show similar surface band structures for the CO adsorption but different adsorption energies, which is explained by the stronger CO 5σ state to the metal d states donation or the effectively screened Pauli repulsion. This work underlines the screening strength as a main difference between sX and HSE06, as well as an important hybrid functional parameter for surface calculation. © *2016 Author(s). All article content, except where otherwise noted, is licensed under a Creative Commons Attribution (CC BY) license (http://creativecommons.org/licenses/by/4.0/).* [http://dx.doi.org/10.1063/1.4954032]

INTRODUCTION

Density functional theory (DFT) has become the standard technique to calculate the electronic structures of materials.[1–3] Its wide application attributes to the general computational accuracy and practical moderate computational cost. The latter is achieved in the Kohn-Sham (KS) wisdom[4] by mapping the many-electron interacting system to an auxiliary non-interacting system with the same ground state electron density. The accuracy of this procedure is taken care of by the proper exchange-correlation (XC) functional. The most widely used XC functionals such as the local density approximation (LDA) and the generalized gradient approximation (GGA) replace the XC energy of the many-electron Schrodinger equation with a functional of the local electron density.[5,6]

[a]Electronic address: li_huanglong@mail.tsinghua.edu.cn
[b]Electronic address: jr214@cam.ac.uk

    6, 065309-1

The LDA and GGA describes the ground state properties such as the lattice constant quite well at low computational cost. However, it is well known that these two functionals underestimate the band gaps of semiconductors and insulators due to the lack of energy discontinuity across the Fermi level as a functional of electron occupancy.[7,8] At the same time, the LDA and GGA are not well suited for the description of strongly correlated systems, partly due to the incomplete self-interaction cancellation.[9] One of the most advanced methods to remedy the drawbacks of the LDA and GGA is the GW method.[10–14] Here, the self-energy of a system is approximated using a Green's function technique with dynamically screened Coulombic interaction. The quasi-particle energy is then obtained by correcting the KS eigenvalues, using the expectation values of the approximated self-energy over each KS orbital. The GW method can achieve accurate band structure description, however, it is prohibitively computationally demanding for applications to complex systems. Therefore, a DFT-style functional of both high accuracy and moderate computational cost is still useful.

The advantages are offered by hybrid functionals, which are a class of functionals that empirically mix a certain percentage of non-local Hartree-Fock (HF) potential with a local XC functional. This is motivated by the fact that pure HF exchange tends to over-estimate the band gaps, while the LDA causes underestimation;[6,7,9] the opposing behaviors thus largely cancel if balanced by suitable mixing scheme. Although more costly than the LDA and GGA, hybrid functionals are substantially less computationally expensive compared to GW method. We apply on two hybrid functionals in this work, which were both found to give accurate description of the band gaps of various systems[15–21]: HSE06[22–24] is one of the most well-known hybrid functionals for use in extended systems. It includes 25% (but tunable) of non-local HF exchange that is screened in long range by an error function $erfc(\omega^*|r - r'|)$, where ω is the screening parameter of HSE06 and $|r - r'|$ is the electron separation. In contrast to HSE06, the screened exchange (sX) functional[25] includes 100% (fixed) of HF exchange and the correlation effect is manifested in screening the HF over a shorter distance. This is achieved by introducing a factor which decays exponentially with electron separation, namely, $\exp(-k_s^*|r - r'|)$, where k_s is the Thomas-Fermi (TF) screening constant. Its contribution to the total energy in a periodic system of plane waves is

$$E_{nl}^{sX} = -\frac{1}{2} \sum_{ij,kq} \int \int \frac{\varphi_{ik}^*(r)\varphi_{ik}(r')\exp(-k_s|r-r'|)\varphi_{jq}^*(r')\varphi_{jq}(r)}{|r-r'|} dr\,dr' \qquad (1)$$

where i and j label electronic bands, k and q are the k points. We also include a local contribution $E_{loc}^{sX}[n(r)]$ to maintain the exact XC energy for the homogeneous electron gas (HEG). This ensures that the sX meets both the LDA and HF limits for the HEG at long and short screening lengths.

$$E_{loc}^{sX}[n(r)] = E^{HEG}[n(r)] - E_{nl}^{HEG}[n(r)] \qquad (2)$$

where the first term on the right is just the LDA functional. The second term is the non-local exchange-correlation energy of the HEG with a density n(r). Combining the local and non-local part gives the full sX exchange-correlation energy,

$$E^{sX}[n(r)] = E_{loc}^{sX}[n(r)] + E_{nl}^{sX}[n(r)] \qquad (3)$$

The TF screening constant represents the screening range of the electron interaction. If $k_s = 0$, the non-local XC becomes the full HF energy and the local part becomes the LDA correlation energy. If k_s is infinite, there is full screening. The HF part is screened away and the XC energy is equal to the local part and pure LDA. Therefore sX gives the correct asymptotic limit of the free electron gas and the screened functional of sX functional is closer to the Coulomb-hole and screened-exchange (COHSEX) in the first-order GW method. Therefore, better performances of the sX functional are anticipated.

In the work by Feibelman,[26] the inability of DFT to correctly predict the atop adsorption site of CO on Pt(111) was outlined, which since then has become a benchmark test for advanced DFT functionals and theories even beyond DFT.[27] According to the low-energy electron diffraction (LEED) and electron energy loss spectroscopy (EELS) analysis,[28–31] CO resides on the atop site of

Pt(111), singly coordinated to one Pt atom. It was noted that increasing the energy difference between the highest occupied molecular orbital (HOMO) and the lowest unoccupied molecular orbital (LUMO) might cure this problem of DFT,[32–34] and that this could be achieved by using hybrid functionals.[33,35–38] However, the B3LYP functional marginally failed to achieve this site preference,[33] as did a study using the HSE06 hybrid functional.[35] A recent work found that the PBEh hybrid functional can give the correct site preference by treating the 5s and 5p states as the core states.[36] Alternatively, inclusion of non-local correlation effects corresponding to dispersion-type van der Waals interactions in density functional[39] and embedded, correlated wavefunction-based method with a kinetic energy density functional approach[40] are reported to improve the prediction of the correct adsorption site. It has also been shown[27] that the random phase approximation (RPA), which is closely connected to the GW method, can give the adsorption energy close to the experimental value and predict the correct atop adsorption site. Recently, screened non-local hybrid density functional with a RPA long range correlation has been proposed.[41,42] Moreover, varying the screening parameter was found to affect the overall accuracy of HSE06 hybrid functional.[43] Therefore, given the wide application and practical moderate computational cost of sX, studying the screening effects of sX is important in its own right and provides useful information for designing new functionals like sX+ RPA which could potentially be interesting. In this work, we thus investigate the screening effects of the screened exchange (sX) hybrid functional in CO adsorption on Pt(111) surfaces.

METHODS

The adsorption geometry of CO on Pt(111) is relaxed in a $(\sqrt{3} \times \sqrt{3})$-R30° supercell containing four layers of metal and 15 of Å vacuum, as shown in Fig. 1. The sX method has been implemented within the planewave basis set and pseudopotential formalisms in the CASTEP code.[44] The valence
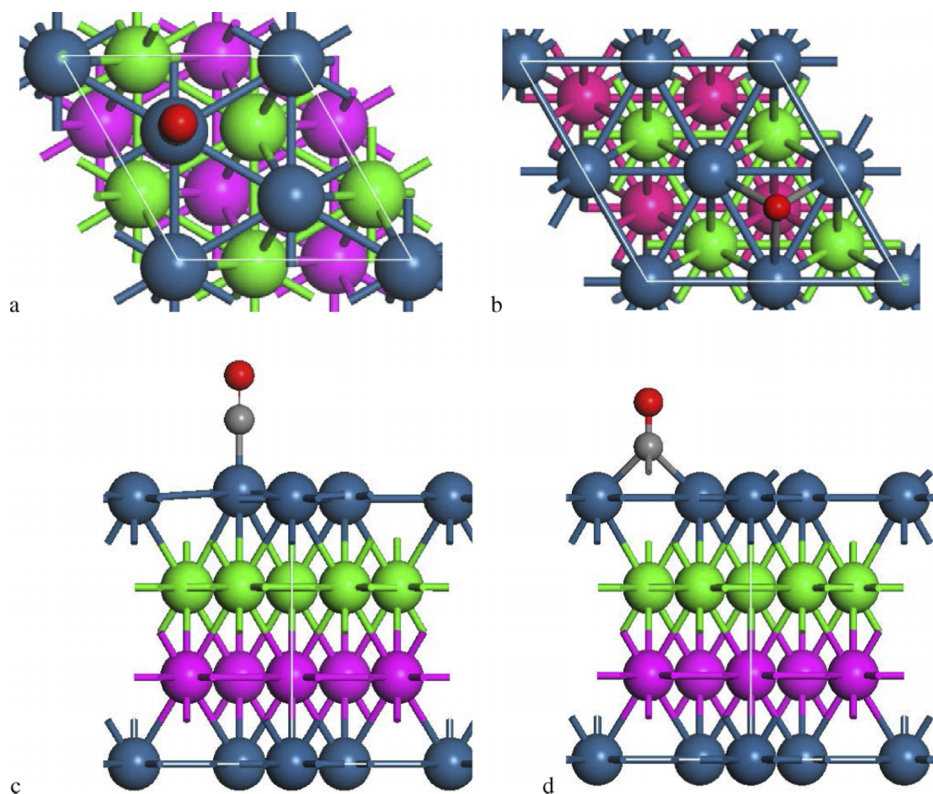

FIG. 1. Top view of the CO adsorption on (a) the atop site and (b) the fcc site of the $(\sqrt{3} \times \sqrt{3})$-R30° Pt(111) or Rh(111) surface; side view of the CO adsorption on (c) the atop site and (d) the fcc site. Big atoms are Pt or Rh, grey atom is C and red atom is O.

electron wave functions are described by a planewave expansion and the ion-electron interactions are described using the norm-conserving pseudopotentials of the Kleinman-Bylander form, treating the 5s and 5p states as core states. Treating the 5s and 5p states explicitly as the valence states was reported.[38] Within the scope of this work, the behavioral differences between the sX functional and HSE06 functional, and the screening effect of the sX functional are reflected in a same functional independent parameterization scheme. A cutoff energy of 1000 eV and a 4x4x1 Monkhorst-Pack K points mesh are used. For the HSE06 functional in this work, we use the same screening parameter as in Ref. 38. The total energy of the supercell is converged to 3×10^{-5} eV. The adsorption energy of CO on Pt(111) is calculated according to equation

$$E_{ads} = E_{CO-Pt111} - E_{CO} - E_{Pt111} \qquad (4)$$

where E_{ads} is the adsorption energy, $E_{CO-Pt111}$ is the total energy of the supercell containing CO on Pt(111), E_{CO} and E_{Pt111} are the total energies of the supercells containing CO and Pt(111) only, respectively. The surface energy of Pt(111) is calculated according to equation

$$E_{surf} = \frac{1}{2}(E_{Pt111} - NE_{bulkPt}) \qquad (5)$$

where E_{surf} is the surface energy, E_{Pt111} is the total energy of the supercell containing Pt(111), E_{bulkPt} is the bulk energy per Pt atom, N is the number of atoms in the Pt(111) supercell. The pre-factor $\frac{1}{2}$ accounts for the fact that there are two identical Pt(111) surfaces in the Pt(111) supercell model. The primitive cell of bulk Pt is relaxed using a 8x8x8 k-point mesh, which has roughly the same Brillouin zone sampling density as in the slab calculation. A four-layer Pt(111) surface model has been adopted in previous works on HSE06[38] and PBE0,[36] respectively, where reasonably good convergence for adsorption energy and surface energy calculations was reported. In order to ensure its adequacy, we perform surface energy calculations on Pt(111) models of six, eight, ten and twelve layers, respectively, by GGA functional in the assumption of similar convergence behaviors between GGA and hybrid functionals, and in the attempt to avoid the larger computational demand of the hybrid functional calculations. We observe decreasing surface energy up to 1×10^{-2} eV/u.a. with increasing number of layers, which is equivalent to 2% surface energy variation and reasonably adequate for purpose of this work. A 4x4x1 k-point mesh has also been adopted for the same slab supercell size in Refs. 36 and 38. where it is reported to be good enough to produce reliable results. In order to ensure the reliability, we perform surface energy calculations on a four-layer Pt(111) model using and 5x5x1, 6x6x1, 7x7x1 k-point meshes, respectively, by GGA functional. To the best of our knowledge, the latter grid is the densest reported Brillouin zone sampling for hybrid functionals applied to this system. We find that the total energy of the Pt(111) slab is well converged to 0.03 eV with respect to the k-point sampling density, resulting in less than 1% surface energy variation which is reasonably good.

RESULTS AND DISCUSSION

We calculate the surface energy of Pt(111) and the CO adsorption energy on different sites of Pt(111). The adsorption energies on the atop site against the surface energies by different functionals are plotted in Fig. 2. Two screening parameters are considered for the sX functional: $k_s = 1.44$ Å^{-1} and $k_s = 2.38$ Å^{-1}, denoted as sX(1.44) and sX(2.38) respectively. The Thomas-Fermi screening parameter in sX functional is proportional to the one sixth root of valence electron density.[45] It has been found that due to the nature of screening and similar valence density in a wide range of solid state materials, the screening parameter generally falls into this range.[45] A larger screening parameter leads to a stronger screening effect. Fig. 2 indicates that the surface energies calculated by both the HSE06 and sX functionals are smaller than the experimental value, *i.e.* over-stabilizing the surface. It would be expected that this would result in too small adsorption energies, however, the contrary is found: Our calculated adsorption energies from both the HSE06 and sX functionals are larger than the experimental value.

Fig. 3 compares the site preferences predicted by the HSE06 and sX functionals. It shows that both the HSE06 and sX functionals predict the correct site preference. It is interesting that for the
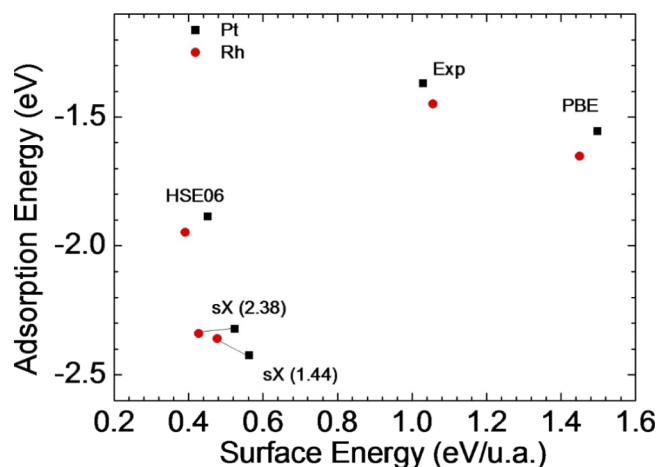
FIG. 2. Adsorption energy on the atop site against surface energy of CO adsorbed on Pt(111) or Rh(111) by the PBE, HSE06 and sX functionals. For the sX, different screening parameters are used for comparison.
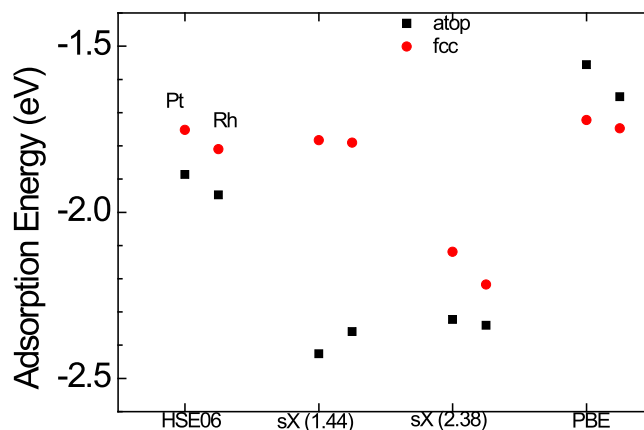

FIG. 3. Adsorption energy on the atop site against adsorption energy on the Pt(111) or Rh(111) fcc site by the PBE, HSE06 and sX functionals. For the sX, different screening parameters are used for comparison.

sX functional, the adsorption energy on the atop site only slightly decreases by 0.10 eV for Pt(111) (we also compare it with Rh(111) system and find 0.02 eV difference for Rh(111) system) with stronger screening effect, while it increases significantly for the fcc site adsorption by 0.34 eV for Pt(111) (0.43 eV for Rh(111)), by changing the screening parameter from 1.44 Å^{-1} to 2.38 Å^{-1}. In the comparison between CO adsorption on Pt(111), it is also noted that the functionals, except for the sX(1.44), predict a preference of the atop binding for Rh over that for Pt, which agrees with Ref. 38 that the preference for the atop binding decreases with increasing d band filling. This is explained in terms of the occupation of the antibonding 5σ-d hybridized states that destabilize the molecular surface bond, in the conventional CO 5σ–metal d states interaction picture. In contrast, the sX(1.44) functional does not predict so. The density of states (DOS) of the surface Pt and the CO molecule on the atop site are plotted in Fig. 4. For the HSE06 functional, the energy levels of the 5σ and 2π* states are well described despite of the slightly lower 2π* state than the experimental value. The 5σ and 2π* energy levels given by the sX(2.38) functional are similar to that given by the HSE06 functional. They both give similar metal d bandwidth, which is overestimated compared to the experiment, as also noted by Ref. 27. On the other hand, the sX(1.44) functional predicts a larger energy gap between the 5σ and 2π* states. The 5σ state lies at larger binding energy compared with experimental value, and the 2π* state is shifted towards vacuum level away from the experimental value. The metal d bandwidth is also further increased for the sX(1.44) functional.
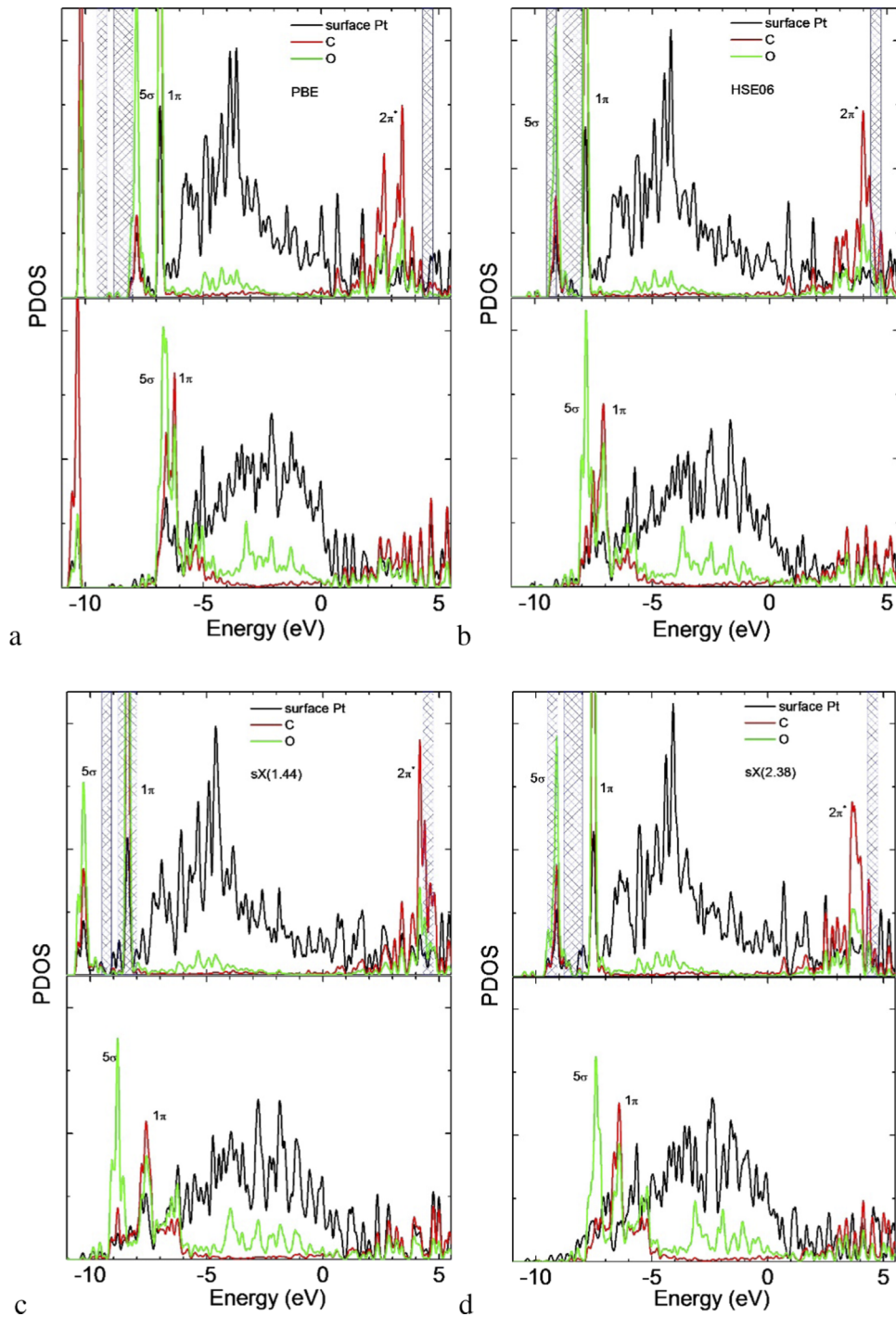
FIG. 4. DOSs of adsorbed CO on the atop (up) and fcc (down) sites of Pt (111) by the (a) PBE, (b) HSE06 and (c), (d) sX functionals. For the sX, different screening parameters are used for comparison. Shaded areas indicates experimental values from[50] and[51] for 5σ, 1π and 2π* states, respectively.

We also show the band structure of the CO adsorbed on the fcc site. For all functionals considered, we find more contribution of O in the interval between the 5σ energy level and the Fermi energy level for the fcc site adsorption than that for the atop site adsorption. This is rationalized as the stronger back-donation effect for the fcc site adsorption,[46] as in the context of the Blyholder

model.[47] Upon CO adsorption, there is significant mixing of the adsorbate 1π and 2π orbitals (the latter accounts for back-donation) with the metal d band, generating three new hybrid π orbitals in an allylic configuration.[48,49] Thus a band is formed by an antibonding 1π and a bonding 2π admixture to the metal d band, leading to a cancellation of orbital amplitude at the carbon and an increase at the oxygen. From the DOS, we also see that the 5σ state lies at lower bonding energy for the fcc site adsorption than that for the atop adsorption as calculated by each functional, respectively. This indicates a weaker interaction (donation) of CO 5σ with metal d states for the fcc site adsorption. The intensity of the $2\pi^*$-d and 5σ-d interactions is in agreement with that from symmetry considerations. Although the HSE06 and sX(2.38) functionals give similar CO/metal(111) band structures, the HSE06 functional gives a smaller adsorption energy for both the atop and fcc adsorption. This is because they have different strengths of CO-metal d states interaction, given their different HOMO-LUMO gaps for isolated CO, as will be shown below.

The calculated HOMO-LUMO gaps of the isolated CO by different functionals are given in Table I. The CO bond length is calculated by the PBE functional and then fixed for the calculation. The isolated CO HOMO-LUMO gaps increase in the sequence of sX(2.38)<HSE06<sX(1.44). Given the nearly identical sX(2.38) and HSE06 band structures of CO on Pt(111), this suggests stronger interaction between CO and metal d states by the sX(2.38) as it induces a stronger down-shift of the 5σ state of CO compared to HSE06 for adsorption. Recent theoretical work[45] pointed out that the decreased screening of the exact exchange in the sX functional leads to an opening of the band gap. The sX(1.44) gives the largest difference of adsorption energies between the atop and fcc adsorption, which is difficult to achieve by other functionals including some approaches by the HSE06.[35] This is closely related to the larger HOMO-LUMO gap of CO from the sX(1.44) that prevents the predominant contribution of back-donation in the bond formation, which is inherently strong for the fcc adsorption[46,52] and becomes more effectively if the CO HOMO-LUMO gap is small.

We also compare the atomization energy of the CO molecule by different functionals, as shown in Table I. We see that the PBE functional predicts a lower energy for breaking a CO bond compared with the hybrid functionals. It is interesting that the sX(2.38) functional gives the largest atomization energy, which indicates the most stable CO. Note that the Pt(111) surface is also predicted to be rather stable by the sX(2.38) among these functionals (second most stable), thus the adsorption energy of CO on the metal surface is expected to be small for the sX(2.38) functional. On the other hand, Fig. 3 shows large adsorption energy by the sX(2.38), in particular for the fcc adsorption. This can be explained by the larger shift of the 5σ state of CO relative to its original energy level in the isolated molecule by the sX(2.38), which implies stronger donation effect from CO 5σ state to metal d states in the standard Blyholder model.[47] From a different perspective by Fohlisch et al,[48,49] CO adsorption on Pt(111) involves π and σ interactions where π interaction is attractive but σ interaction is repulsive and they partially compensate each other. The repulsion between CO σ system and the metal s band is minimized by intermixing the σ orbitals and shifting the 5σ state to larger binding energy. Accordingly, the sX(2.38) effectively reduces the repulsion by larger downward shift of the 5σ state, the adsorption energy is therefore large. Interestingly, this can also be interpreted as the screening reducing the strength of the electronic repulsion. The sX(2.38) has the strongest screening among the functionals studied here, as will be shown later.

Now consider the sX(1.44), the HOMO-LUMO of isolated CO is also the largest and the $2\pi^*$ state shifts to the vacuum most, which generally decreases the adsorption energy, with stronger

TABLE I. Calculated values by different functionals of CO HOMO-LUMO gap, CO atomization energy and Pt (111) work function.

	HSE06	PBE	sX(1.44)	sX(2.38)	Exp
CO HOMO-LUMO Gap (eV)	8.2	6.5	9.2	7.8	~11.9 (on Pt)[50,51,53,54]
Atomization Energy (eV)	-16.5	-15.2	-16.1	-16.7	-11.1
Pt Work Function (eV)	5.9	5.7	6.2	6.1	5.7[55]

effect for the fcc site than for the atop site. This fact disfavours the atop adsorption for the sX(1.44) to that for the sX(2.38). However, the sX(1.44) also gives more unstable isolated CO and Pt(111) surface. This promotes the atop adsorption. As the result of these two competing effects, the adsorption energy for the atop site is still larger for the sX(1.44) than that for the sX(2.38) as shown in Fig. 3. The fcc adsorption energy, on the other hand, is decreased significantly due to the strongly reduced metal d states to CO $2\pi^*$ state back-donation effect.

The behavior of the sX functional in the CO/Pt(111) system must be rooted in the intrinsic functional properties. Inclusion of the HF potential and screening of the HF potential are the most prominent features of the sX and HSE06 hybrid functionals. Fig. 5 compares the fraction of the HF potential kernel ($\propto \frac{1}{r}$) in different functionals. The HF potential in sX functional is Thomas-Fermi screened and the fraction of the HF potential decreases in an exponential manner with respect to distance according to exp(-k_s*r), as labelled in the figure. While for the HSE06 functional, the HF potential is screened by an error function erfc(r) that the fraction of the HF potential decreases with respect to distance according to 0.25*erfc(r), where the pre-factor 0.25 accounts for the mixing percentage. Here, it is easier to treat the mixing percentage (HF fraction at r=0) of HF potential and the screening parameter as two independent functional parameters, as in Ref. 43. By doing so, we are able to define the "screening strength" as follows, which is directly comparable among sX, HSE06 and GGA, regardless of the mixing percentage of HF potential. The absolute value of the slope of the HF fraction curve as a function of the distance reflexes the strength of screening, namely, how fast the fraction of HF potential decays with distance. We first summarize the effects of screening strength. It can be seen that the strength of screening increases in the sequence of HSE06<sX(1.44)<sX(2.38). Note that GGA has no HF and screening included. As has been discussed above, the effects of screening are at least two-fold: first, the HOMO-LUMO gap is screening strength dependent. The site preference is most affected by this factor. The sX(1.44) gives the largest HOMO-LUMO gap for the isolated CO molecule. The adsorption energy difference between the atop and fcc site is also the largest by the sX(1.44) which is explained by the reduced metal d states to the CO $2\pi^*$ state back-donation, with stronger effect for the fcc adsorption than for the atop adsorption; second, the absolute value of the adsorption energy is screening strength dependent, as is clear by comparing the sX(2.38) and HSE06 which give similar band structures but have large screening strength difference. The larger adsorption energy by sX(2.38) than HSE06 can be understood by the stronger CO 5σ state to the metal d states donation or mitigation of the electronic repulsion by the stronger screening. By comparing HSE06 and GGA functionals, Stroppa et al[38] found that for atop adsorption, the HSE06 adsorption energies are larger than the GGA ones. This was interpreted by the suppression of charge depletion from surface layer to
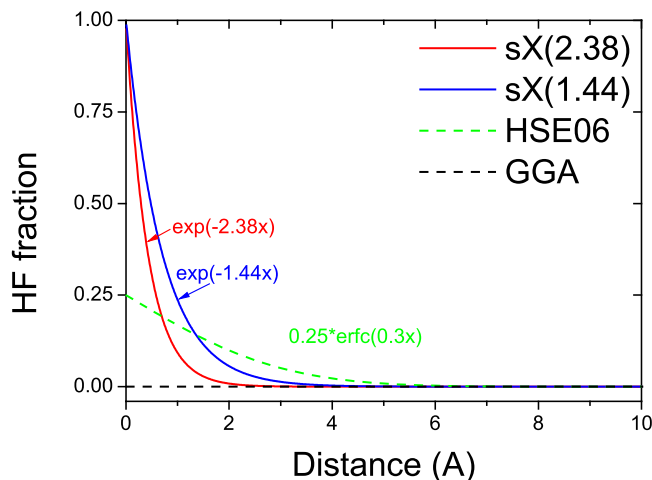

FIG. 5. Comparison of the HF fraction in different functionals. The screening kernels of respective functionals are indicated.

vacuum by HSE06, which reduces the steric repulsion. We here provide an alternative explanation based on the nature of screening: the stronger screening provided by HSE06, the weaker the Coulombic (steric) repulsion. Moussa et al[43] found that by using a single ω value in erfc(ω r) of HSE06 with 0.95 HF mixing percentage, the sX(k_s) band gaps for various semiconductors can be reproduced; but the ω value has to be large, indicating stronger screening strength than normal HSE06 is required. This further underlines the difference between sX and HSE06 in terms of the screening strength which is an important hybrid functional parameter for both bulk and surface calculations. Despite of the correct site preference predicted by the hybrid functional in this work, both of the adsorption energy and the surface energy have discrepancy with the experimental values, which is a known failure of the hybrid functional.[27,38]

The possible effects of different mixing percentage of HF potential of the sX and HSE06 still cannot be ruled out. In terms of pure metal surfaces, Soini et al[56] found that the smaller HF mixing percentage in the TPSSh hybrid functional, compared with 20% HF in B3LYP and 25% HF in PBE0, offers a reasonable compromise between the self-interaction corrections and static correlation that it yields an overall good description of the late transition metal clusters. In terms of CO adsorbate on Pt(111) surface, Ref. 36 reported correct site preference based on the PBE0 functional which has no screening; on the other hand, GGA is found not able to get the right answer and it has no screening either. The difference may therefore come from a different HF mixing percentage. The HF mixing percentage can have the same effect as the screening strength in terms of tuning the HOMO-LUMO gap. It is noteworthy that the sX includes 100% of Hartree-Fock exchange (at r=0), compared with 25% of the HSE06. The sX also has more relevant screened potential as the GW. Further case studies on the CO/Pt(111) problem by varying the HF mixing percentage in HSE06 might be useful to identify other HF mixing percentage dependent functional behaviors.

CONCLUSIONS

The effects of screening parameter of sX are studied in CO adsorption on Pt(111) surface. The sX(1.44) functional gives the largest CO HOMO-LUMO gap which tends to reduce the back-donation effect for the fcc adsorption more effectively than that for the atop adsorption. As a result, the sX(1.44) functional predicts the largest difference of adsorption energy on the atop and fcc sites. The difference between the sX(2.38) and HSE06 is explained by a stronger donation effect of the sX(2.38) or effectively screened Pauli repulsion, which is rooted in their difference of screening strength. Therefore, two effects of the screening are extracted from these results: first, the HOMO-LUMO gap is screening dependent. This affects the site preference most significantly; second, the adsorption energy is screening dependent. This work underlines the screening strength as a main difference between sX and HSE06, as well as an important hybrid functional parameter for surface calculation. The effects of another independent parameter, e.g. the mixing percentage of HF potential, is subject to further study. This work provides useful insights into the screening dependent behaviors of the sX applied to surface systems.

ACKNOWLEDGMENTS

[1] W. Kohn, A. D. Becke, and R. G. Parr, J. Phys. Chem. **100**, 12974 (1996).
[2] Y. Zhao, N. E. Schultz, and D. G. Truhlar, J. Chem. Theory Comput. **2**, 364 (2006).
[3] M. C Payne, M. P. Teter, D. C. Allan, T. A. Arias, and J. D. Joannopoulos, Rev. Mod. Phys. **64**, 1045 (1992).
[4] W. Kohn and L. J. Sham, Phys. Rev **140**, A1133 (1965).
[5] J. P. Perdew, K. Burke, and M. Ernzerhof, Phys. Rev. Lett. **77**, 3865 (1996).
[6] A. D. Becke, Phys. Rev. A **38**, 3098 (1988).
[7] L. J. Sham and M. Schluter, Phys. Rev. Lett. **51**, 1888 (1983).

[8] J. P. Perdew and M. Levy, Phys. Rev. Lett. **51**, 1884 (1983).

[9] P. Mori-Sanchez, A. J. Cohen, and W. Yang, Phys. Rev. Lett. **100**, 146401 (2008).

[10] M. Hybertsen and S. G. Louie, Phys. Rev. B **34**, 5390 (1986).

[11] F. Aryasetiawan and O. Gunnarsson, Rep. Prog. Phys. **61**, 237 (1998).

[12] M. van Schilfgaarde, T. Kotani, and S. Faleev, Phys. Rev. Lett. **96**, 226402 (2006).

[13] M. Shishkin and G. Kresse, Phys. Rev. B **75**, 235102 (2007).

[14] H. Jiang, P. Rinke, and M. Scheffler, Phys. Rev. B **86**, 125115 (2012).

[15] J. Heyd and G. E. Scuseria, J. Chem. Phys. **121**, 1187 (2004).

[16] J. Heyd, J. E. Peralta, E. Scuseria, and R. L. Martin, J. Chem. Phys. **123**, 174101 (2005).

[17] J. Paier, M. Marsman, K. Hummer, G. Kresse, I. C. Gerber, and J. G. Angyan, J. Chem. Phys. **124**, 154709 (2006).

[18] W. Chen and A. Pasquarello, Phys. Rev. B **86**, 035134 (2012).

[19] S. J. Clark and J. Robertson, Phys. Rev. B **82**, 085208 (2010).

[20] R. Gillen, S. J. Clark, and J. Robertson, Phys. Rev. B **87**, 125116 (2013).

[21] Y. Guo, S. J. Clark, and J. Robertson, J. Chem. Phys. **140**, 054702 (2014).

[22] J. Heyd, G. E. Scuseria, and M. Ernzerhof, J. Chem. Phys. **118**, 8207 (2003).

[23] A. V. Krukau, O. A. Vydrov, A. F. Izmaylov, and G. E. Scuseria, J. Chem. Phys. **125**, 224106 (2006).

[24] J. E. Peralta, J. Heyd, G. E. Scuseria, and R. L. Martin, Phys. Rev. B **74**, 073101 (2006).

[25] D. M. Bylander and L. Kleinman, Phys. Rev. B **41**, 7868 (1990).

[26] P. Feibelman, B. Hammer, J. K. Nørskov, F. Wagner, M. Scheffler, R. Stumpf, R. Watwe, and J. Dumesic, J. Phys. Chem. B **105**, 4018 (2001).

[27] L. Schimka, J. Harl, A. Stroppa, A. Gruneis, M. Marsman, F. Mittendorfer, and G. Kresse, Nat. Mater. **9**, 741 (2010).

[28] D.F. Ogletree, M.A. Van Hove, and G.A. Somorjai, Surf. Sci. **173**, 351 (1986).

[29] G. S. Blackman, M. -L. Xu, D. F. Ogletree, M. A. Van Hove, and G. A. Somorjai, Phys. Rev. Lett. **61**, 2352 (1988).

[30] H. Steininger, S. Lehwald, and H. Ibach, Surf. Sci. **123**, 264 (1982).

[31] H. Hopster and H. Ibach, Surf. Sci. **77**, 109 (1978).

[32] G. Kresse, A. Gil, and P. Sautet, Phys. Rev. B **68**, 073401 (2003).

[33] A. Gil, A. Clotet, J. M. Ricart, G. Kresse, M. Garcia-Hernandez, N. Rösch, and P. Sautet, Surf. Sci. **530**, 71 (2003).

[34] S. E. Mason, I. Grinberg, and A. M. Rappe, Phys. Rev. B **69**, 161401 (2007).

[35] A. Stroppa, K. Termentzidis, J. Paier, G. Kresse, and J. Hafner, Phys. Rev. B **76**, 195440 (2007).

[36] Y. Wang, S. de Gironcoli, N. S. Hush, and J. R. Reimers, J. Am. Chem. Soc. **129**, 10402 (2007).

[37] Q. M. Hu, K. Reuter, and M. Scheffler, Phys. Rev. Lett. **98**, 176103 (2007).

[38] A. Stroppa and G. Kresse, New J. Phys. **10**, 063020 (2008).

[39] P. Lazić, M. Alaei, N. Atodiresei, V. Caciuc, R. Brako, and S. Blügel, Phys. Rev. B **81**, 045401 (2010).

[40] C. Huang, M. Pavone, and E. Carter, J. Chem. Phys. **134**, 154110 (2011).

[41] B. G. Janesko, T. M. Henderson, and G. E. Scuseria, J. Chem. Phys. **131**, 034110 (2009).

[42] J. Paier, B. G. Janesko, T. M. Henderson, G. E. Scuseria, A. Grüneis, and G. Kresse, J. Chem. Phys. **132**, 094103 (2010).

[43] J. E. Moussa, P. A. Schultz, and J. R. Chelikowsky, J. Chem. Phys. **136**, 204112 (2012).

[44] S. J. Clark, M. D. Segall, C. J. Pickard, P. J. Hasnip, M. J. Probert, K. Refson, and M. C. Payne, Z. Kristallogr. **220**, 567 (2005).

[45] Y. Guo, J. Robertson, and S. J. Clark, J. Phys. Cond. Matt. **27**, 025501 (2014).

[46] R. A. Van Santen, J. Chem. Soc. Faraday Trans. **83**, 1915 (1987).

[47] G. J. Blyholder, J. Phys. Chem. **68**, 2772 (1964).

[48] A. Fohlisch, M. Nyberg, J. Hasselström, O. Karis, L. G. M. Pettersson, and A. Nilsson, Phys. Rev. Lett. **85**, 3309 (2000).

[49] A. Fohlisch, M. Nyberg, P. Bennich, L. Triguero, J. Hasselström, O. Karis, L. G. M. Pettersson, and A. Nilsson, J. Chem. Phys. **112**, 1946 (2000).

[50] T. Anazawa, I. Kinoshita, and Y. Matsumoto, J. Electron Spectrosc. Relat. Phenom. **88**, 585 (1998).

[51] G. Tsilimis, J. Kutzner, and H. Zacharias, Appl. Phys. A **76**, 743 (2003).

[52] P. Hu, D. A. King, M. H. Lee, and M. C. Payne, Chem. Phys. Lett. **246**, 73 (1995).

[53] V. Dose, J. Rogozik, A. M. Bradshaw, and K. C. Prince, Surf. Sci. **179**, 90 (1987).

[54] G. Rangelov, N. Memmel, E. Bertel, and V. Dose, Surf. Sci. **251**, 965 (1991).

[55] H. L. Skriver and N. M. Rosengaard, Phys. Rev. B **46**, 7157 (1992).

[56] T. M. Soini, A. Genest, A. Nikodem, and N. Rösch, J. Chem. Theory Comput. **10**, 4408 (2014).